Saturation mechanism of the fluctuation dynamo at $\mathrm{Pr}_M \geqslant 1$

Amit Seta,[1,2,*] Paul J. Bushby,[2] Anvar Shukurov,[2] and Toby S. Wood[2]
[1]*Research School of Astronomy and Astrophysics, Australian National University, Canberra ACT 2611, Australia*
[2]*School of Mathematics, Statistics and Physics, Newcastle University, Newcastle Upon Tyne NE1 7RU, United Kingdom*

(Received 28 October 2019; accepted 17 March 2020; published 21 April 2020)

The presence of magnetic fields in many astrophysical objects is due to dynamo action, whereby a part of the kinetic energy is converted into magnetic energy. A turbulent dynamo that produces magnetic field structures on the same scale as the turbulent flow is known as the fluctuation dynamo. We use numerical simulations to explore the nonlinear, statistically steady state of the fluctuation dynamo in driven turbulence. We demonstrate that as the magnetic field growth saturates, its amplification and diffusion are both affected by the back-reaction of the Lorentz force upon the flow. The amplification of the magnetic field is reduced due to stronger alignment between the velocity field, magnetic field, and electric current density. Furthermore, we confirm that the amplification decreases due to a weaker stretching of the magnetic field lines. The enhancement in diffusion relative to the field line stretching is quantified by a decrease in the computed local value of the magnetic Reynolds number. Using the Minkowski functionals, we quantify the shape of the magnetic structures produced by the dynamo as magnetic filaments and ribbons in both kinematic and saturated dynamos and derive the scalings of the typical length, width, and thickness of the magnetic structures with the magnetic Reynolds number. We show that all three of these magnetic length scales increase as the dynamo saturates. The magnetic intermittency, strong in the kinematic dynamo (where the magnetic field strength grows exponentially), persists in the statistically steady state, but intense magnetic filaments and ribbons are more volume-filling.

DOI: 10.1103/PhysRevFluids.5.043702

I. INTRODUCTION

Magnetic fields are observed in a variety of astrophysical objects, including stars, galaxies, and galaxy clusters, where they play an important role in various physical processes. Based on length and timescales, astrophysical magnetic fields can be divided into two types: the large scale or mean field, which is coherent over scales comparable to the size of the system, and the small scale or fluctuating field, whose correlation length is of the order of the driving scale of the underlying turbulent flow. The driving scale of turbulence, l_0, is of the order of 0.1 kpc in spiral galaxies [1–3], and 10 kpc in galaxy clusters [4,5]. The fluctuating magnetic field is believed to evolve over the eddy turnover timescale, which is considerably shorter than the corresponding evolution timescale for the large-scale field (which is typically of the order of 10^8 yr in spiral galaxies, comparable to the rotation period). For spiral galaxies, the mean and fluctuating fields have comparable magnitudes and thus both kinds of fields are equally important for the galactic dynamics [6]. There are a number of reviews covering the theoretical, numerical, and observational aspects of the subject [7–12].

*amit.seta@anu.edu.au

The evolution and maintenance of magnetic fields is generally explained by dynamo action, a process by which kinetic energy is converted to magnetic energy. Astrophysical flows leading to dynamo action are typically turbulent; such flows may be driven by convection in stars, supernovae in galaxies, and merger shocks, motion of galaxies and AGN outflows in galaxy clusters. Magnetic field amplification by turbulent motions has also been observed in laboratory experiments [13]. Depending upon the magnetic fields that they produce, such dynamos are generally categorized as either mean-field or fluctuation (or "small-scale") dynamos. Mean-field dynamos produce large-scale magnetic fields, whereas the fluctuation dynamo generates the small-scale component of the field via random stretching of field lines by the turbulent velocity [14,15] (as conceptually explained by the stretch-twist-fold mechanism [16,17]). Fluctuation dynamo action plays a crucial role not only in spiral galaxies [7,10,18–21], elliptical galaxies [22,23], and galaxy clusters [24–27] but also in stars such as the Sun [28–31], making it a general type of astrophysical process. Fluctuation dynamos naturally produce intermittent magnetic fields [32–34], characterized by the presence of intense, localized field structures. In the galactic context, a better understanding of these structures is needed for cosmic ray propagation studies [35,36] and in the galaxy cluster context for the interpretation of radio observations [37]. The initial stages of magnetic field growth, when the Lorentz force is negligible, have been thoroughly studied [9,32], so here we focus on the nonlinear states of the fluctuation dynamo, for which it is possible to consider relatively simple idealized flows (i.e., homogeneous, isotropic turbulence). A mean-field dynamo would require additional physics, such as rotation, velocity shear, and density stratification; such effects can be safely ignored over the length and timescales that will be of interest here.

In a fluctuation dynamo, the root-mean-square (rms) magnetic field grows exponentially if the magnetic Reynolds number Re_M (quantifying the efficiency of inductive effects compared to magnetic diffusion) exceeds its critical value $\mathrm{Re}_M^{(\mathrm{crit})}$, which depends on the properties of the flow. When the magnetic energy is low in comparison to the turbulent kinetic energy, the flow dynamics are not influenced by the magnetic field (the kinematic stage). For an isotropic, incompressible, mirror-symmetric, homogeneous, and Gaussian random velocity field, which is also δ-correlated in time, it can be shown that the magnetic field power spectrum M_k in the kinematic stage follows a power law (at low wave numbers) with slope $3/2$ [9,14]. However, an exponentially growing magnetic field also leads to the exponential growth of the Lorentz force, which eventually makes the problem nonlinear. This slows down the growth and finally leads to the saturation of the dynamo (the saturated stage). The nonlinear problem is mostly studied via numerical simulations, in which the Navier-Stokes and induction equations are solved simultaneously [e.g., 26,28,30,33,38–47]. Our aim in this paper is to explore the saturation mechanism of the fluctuation dynamo and to characterize the magnetic structures it generates.

For fluctuation dynamos driven by homogeneous and isotropic turbulence, the following three quantities are prescribed: the driving scale of the turbulent flow l_0, the fluid viscosity ν, and the magnetic resistivity η. Based on the magnetic Prandtl number Pr_M (defined to be the ratio of viscosity to resistivity, $\mathrm{Pr}_M = \nu/\eta$), fluctuation dynamos can be divided into small and large Pr_M cases. Pr_M is greater than unity ($\eta < \nu$) for hot diffuse plasma (interstellar and intergalactic medium) and Pr_M is much smaller than unity ($\eta > \nu$) for dense plasma (planets, stars, and liquid metal dynamo experiments). The critical magnetic Reynolds number $\mathrm{Re}_M^{(\mathrm{crit})}$, which is a threshold for dynamo action to occur, increases with decreasing Pr_M [48–52]. We focus upon the $\mathrm{Pr}_M \geqslant 1$ regime, fixing the underlying flow (i.e., fixing Re) and then varying Re_M to study the sensitivity of the magnetic structures of nonlinear dynamo states to the magnetic Reynolds number.

This paper is structured as follows. In Sec. II, we introduce the basic equations and describe the numerical setup and provide parameters of the simulations. In Sec. III, we discuss magnetic field intermittency. In Sec. IV, we examine possible saturation mechanisms. In Sec. V, we use Minkowski functionals to quantify the magnetic field structures (as a function of the magnetic Reynolds number) in both the kinematic and nonlinear regimes. Finally, in Sec. VI, we conclude with a discussion and propose some future directions of research.

II. BASIC EQUATIONS AND NUMERICAL MODELLING

To study the fluctuation dynamo action in a turbulent flow driven by a prescribed random force, we solve the equations of magnetohydrodynamics, using the Pencil code [53]. The computational domain is a triply periodic cubic box of nondimensional width $L = 2\pi$, with 256^3 or 512^3 grid points. The equations are solved with sixth-order finite differences in space and a third-order Runge–Kutta scheme for the temporal evolution. The governing equations are

$$\frac{\partial \rho}{\partial t} + \nabla \cdot (\rho \mathbf{u}) = 0, \tag{1}$$

$$\frac{\partial \mathbf{b}}{\partial t} = \nabla \times (\mathbf{u} \times \mathbf{b}) + \eta \nabla^2 \mathbf{b}, \tag{2}$$

$$\frac{\partial \mathbf{u}}{\partial t} + (\mathbf{u} \cdot \nabla)\mathbf{u} = -\frac{\nabla p}{\rho} + \frac{\mathbf{j} \times \mathbf{b}}{c\rho} + \nu\left(\nabla^2 \mathbf{u} + \frac{1}{3}\nabla(\nabla \cdot \mathbf{u}) + 2\mathbf{S} \cdot \nabla \ln \rho\right) + \mathbf{F}, \tag{3}$$

where $\mathbf{u}$ is the velocity field, $\mathbf{b}$ is the magnetic field, ρ is the fluid density, p is the pressure, η is the magnetic diffusivity, $\mathbf{j} = (c/4\pi)\nabla \times \mathbf{b}$ is the electric current density, c is the speed of light, ν is the viscosity, $S_{ij} = \frac{1}{2}(u_{i,j} + u_{j,i} - \frac{2}{3}\delta_{ij}\nabla \cdot \mathbf{u})$ is the rate-of-strain tensor, and $\mathbf{F}$ is the forcing function (defined below). We use an isothermal equation of state, $p = c_s^2 \rho$, where the constant c_s is the sound speed. Eq. (2) is solved in terms of the magnetic vector potential to ensure that the magnetic field remains divergence free.

We drive the flow with a mirror-symmetric and δ-correlated in time forcing [39] of the form

$$\mathbf{F}(\mathbf{x}, t) = \mathrm{Re}\{N \mathbf{F}_{\mathbf{k}(t)} \exp[i\mathbf{k}(t) \cdot \mathbf{x} + i\phi(t)]\}, \tag{4}$$

where $\mathbf{k}$ is the wave vector, $\mathbf{x}$ is the position vector and $-\pi < \phi \leqslant \pi$ is a random phase. To ensure that the forcing is nearly δ-correlated in time, $\mathbf{k}$ and ϕ are changed at each time step δt. Also, to ensure that the time-integrated force is independent of the chosen time step δt, the normalization is $N = F_0 c_s (|\mathbf{k}| c_s / \delta t)^{1/2}$, where F_0 is the nondimensional forcing amplitude chosen such that the maximum Mach number is small enough ($u_{\mathrm{rms}}/c_s \lesssim 0.1$) to avoid strong compressibility. We select many random wave vectors $\mathbf{k}$, each of magnitude k (a multiple of $2\pi/L$ to make sure that the flow is periodic) in a given range. Then we select an arbitrary unit vector $\mathbf{e}$ (neither parallel nor anti-parallel to $\mathbf{k}$) and set

$$\mathbf{F}_{\mathbf{k}} = \frac{\mathbf{k} \times \mathbf{e}}{|\mathbf{k} \times \mathbf{e}|}. \tag{5}$$

The form of Eq. (5) ensures that the forcing is solenoidal, i.e., $\nabla \cdot \mathbf{F} = 0$ by construction. The average wave number at which the flow is driven is denoted by k_{F}. Even when the flow is periodic, k_{F} need not be a multiple of $2\pi/L$. Physically, $2\pi/k_{\mathrm{F}}$ represents the driving scale of the turbulent flow, l_0, in the system.

The turbulent plasma is characterized by the hydrodynamic Reynolds number Re and magnetic Reynolds number Re_M, defined in terms of the rms velocity u_{rms} and the forcing scale k_{F} [54], as

$$\mathrm{Re} = \frac{u_{\mathrm{rms}}}{\nu}\frac{2\pi}{k_{\mathrm{F}}}, \quad \mathrm{Re}_M = \frac{u_{\mathrm{rms}}}{\eta}\frac{2\pi}{k_{\mathrm{F}}}. \tag{6}$$

We use nondimensional units with lengths in units of the domain size $L = 2\pi$, speed in units of the isothermal sound speed c_s, time in units of the eddy turnover time $t_0 = 2\pi/u_{\mathrm{rms}} k_{\mathrm{F}}$, density in units of the initial density ρ_0, and the magnetic field in units of $(4\pi\rho_0 c_s^2)^{1/2}$. Initially, the density is constant everywhere and $\mathbf{u} = \mathbf{0}$, while there is a weak random, seed magnetic field with zero net flux across the domain.

TABLE I. Summary of fluctuation dynamo simulations in a numerical domain of size $(L = 2\pi)^3$ with 256^3 mesh points. In all cases, the forcing scale k_F is approximately equal to $1.5(2\pi/L)$, the forcing amplitude $F_0 = 0.02$, the magnetic Prandtl number $\mathrm{Pr}_M = 1$, and the rms velocity in the saturated state is $u_{\rm rms}/c_s \approx 0.11$. For each simulation, we quote the Reynolds number, the magnetic Reynolds number, the rms magnetic field in the saturated state $b_{\rm rms}$, the ratio of magnetic to kinetic energy in the saturated state $\varepsilon_{\rm M}/\varepsilon_{\rm K} = b_{\rm rms}^2/u_{\rm rms}^2$, the correlation length of the velocity and magnetic field in the kinematic stage $l_{u\rm kin}$ and $l_{b\rm kin}$, and similarly in the saturated stage $l_{u\rm sat}$ and $l_{b\rm sat}$.

η, ν	Re_M, Re	$b_{\rm rms}$	$\varepsilon_{\rm M}/\varepsilon_{\rm K}$	$l_{u\rm kin}$	$l_{b\rm kin}$	$l_{u\rm sat}$	$l_{b\rm sat}$
10×10^{-4}	449	0.033	0.08	3.14	1.82	3.77	1.95
5×10^{-4}	898	0.042	0.14	3.20	1.26	3.45	1.76
4×10^{-4}	1122	0.048	0.20	3.01	0.94	3.64	1.76
3×10^{-4}	1496	0.049	0.21	3.01	0.88	3.39	1.57
2.5×10^{-4}	1796	0.054	0.25	2.95	0.75	3.58	1.57
2×10^{-4}	2244	0.055	0.26	2.95	0.69	3.33	1.56

For the first set of simulations, with parameters given in Table I, the turbulent motions are driven at the wave numbers $2\pi/L$ and $2(2\pi/L)$ at equal intensities, which implies that $k_F \approx 1.5(2\pi/L)$. The magnetic field grows for $\mathrm{Re}_M \geqslant \mathrm{Re}_M^{(\rm crit)}$, with $\mathrm{Re}_M^{(\rm crit)} \approx 220$ for $\mathrm{Pr}_M = 1$ [39]. The evolution of the rms velocity field, $u_{\rm rms}$, and magnetic field, $b_{\rm rms}$, is shown in Fig. 1 for $\mathrm{Re}_M = 1122$. The flow speed is controlled by the forcing function and thus remains nearly constant. The magnetic field first decays until it reaches an eigenstate of the induction equation. Then it grows exponentially in the kinematic stage at the growth rate of $0.4\, u_{\rm rms} k_F/2\pi$ in dimensional units. As it becomes stronger, the Lorentz force affects the flow and slows down the exponential increase. Finally, when the magnetic field becomes strong enough, the dynamo reaches a statistically steady state in the saturated stage. The exponential growth and then saturation of the magnetic field occurs in all of the runs shown in Table I.

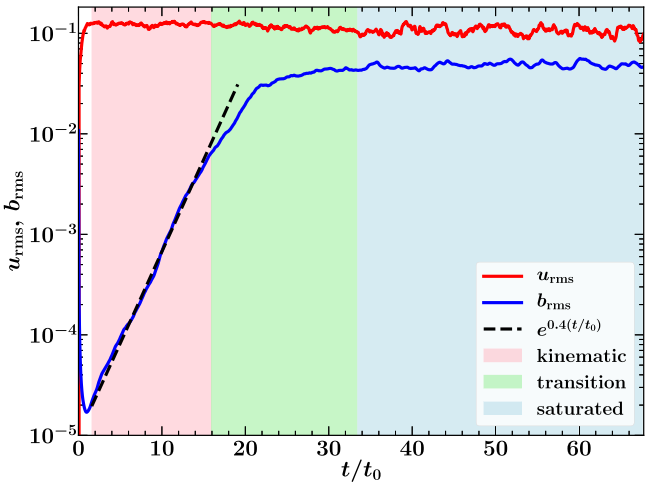

FIG. 1. Root-mean-square (rms) velocity field $u_{\rm rms}$ (red) and magnetic field $b_{\rm rms}$ (blue) as functions of normalized time t/t_0 (where $t_0 = 2\pi/u_{\rm rms}k_F$ is the eddy turnover time) for $\mathrm{Re} = \mathrm{Re}_M = 1122$. During the kinematic stage (area shaded in light red), the black dashed line corresponds to the exponential growth. As the magnetic field grows, the dynamo passes through a transitional stage (area shaded in light green), before reaching a statistically steady saturated state (area shaded in light blue).

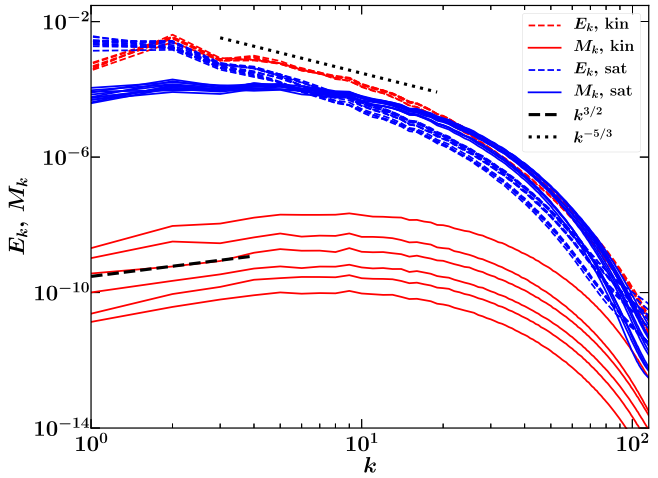

FIG. 2. The shell-averaged (one-dimensional) kinetic E_k (dashed) and magnetic M_k (solid) energy spectra in the kinematic (red) and saturated (blue) stages for $\mathrm{Re} = \mathrm{Re}_M = 1122$. The kinetic energy spectrum is close to the Kolmogorov spectrum, $E_k \propto k^{-5/3}$ (dotted, black) in the main part of the wave number range. The magnetic spectrum is initially of the form $M_k \propto k^{3/2}$ (dashed, black) at smaller wave numbers. As the magnetic field saturates, its power shifts to smaller wave numbers and the magnetic spectrum flattens.

The shell-averaged (one-dimensional) power spectra, for various stages of the magnetic field evolution, are shown in Fig. 2. At all times, the kinetic energy spectrum is close to the Kolmogorov spectrum, $E_k \propto k^{-5/3}$, in the range $3 \leqslant kL/2\pi \leqslant 20$ (flow is driven at $k = 2\pi/L$ and $k = 2(2\pi/L)$), which suggest that the velocity field is turbulent in nature. The magnetic spectrum in the kinematic stage has a broad maximum at large wave numbers and its slope agrees with the Kazantsev model, $M_k \propto k^{3/2}$, in the range $2 \leqslant kL/2\pi \leqslant 10$ with maximum power at approximately $kL/2\pi = 10$. Kazantsev's theory assumes that the turbulent flow is δ-correlated in time. While we have used a δ-correlated forcing in the Navier-Stokes equation [term $\mathbf{F}$ in Eq. (3)], the flow that it drives is not δ-correlated, especially at high Re. However, it is known that the slope of the spectrum in the kinematic stage remains the same even when the flow has a finite but small correlation time [55,56], which explains why we recover the Kazantsev result in these simulations. As the magnetic field grows, the spectral maximum shifts to smaller wave numbers and the spectrum becomes much flatter with a broad maximum in the range $2 \leqslant kL/2\pi \leqslant 5$.

III. MAGNETIC INTERMITTENCY

Intermittency in a random field can manifest itself via heavy tails in its probability distribution function (PDF) and leads to an increased kurtosis in comparison with the Gaussian distribution. For the random velocity field $\mathbf{u}$ with zero mean, the kurtosis is defined by

$$\mathrm{K}(\mathbf{u}) = \frac{\langle \mathbf{u}^4 \rangle}{\langle \mathbf{u}^2 \rangle^2}, \tag{7}$$

with angular brackets denoting the volume average. A useful diagnostic of the spatial structure is the correlation length of the field, l_u, which is calculated from the power spectrum E_k as

$$l_u = \frac{\pi}{2} \frac{\int_0^\infty 2\pi k^{-1} E_k \, dk}{\int_0^\infty E_k \, dk}. \tag{8}$$

Here, using such tools, we discuss the spatial intermittency of the velocity and magnetic fields in nonlinear fluctuation dynamos.

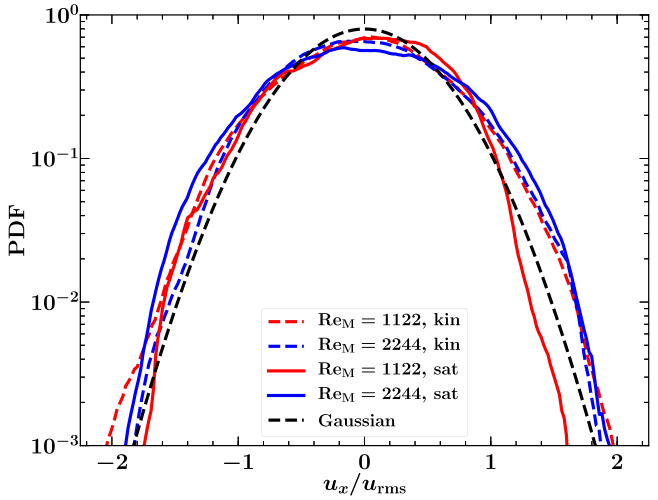

FIG. 3. The PDF of the normalized velocity field component $u_x/\,u_{\rm rms}$ for $\mathrm{Re}_M = 1122$ and $\mathrm{Re}_M = 2244$ in the kinematic (dashed) and saturated (solid) stages for the value of Re_M given in the legend. The PDF of the single component of the velocity field is roughly Gaussian (dashed, black) in both the stages for both Re_M. Here only $u_x/\,u_{\rm rms}$ is shown but similar behavior is exhibited by all three velocity components.

Figure 3 shows the PDF of a single component of the velocity field $u_x/\,u_{\rm rms}$ in the kinematic and saturated dynamo stages for $\mathrm{Re}_M = 1122$ and $\mathrm{Re}_M = 2244$. The PDF is nearly Gaussian in both the kinematic and saturated stages. This is generally true for homogenous turbulence [57]. The velocity PDFs remain Gaussian even in the case of supersonic turbulence with a compressible forcing (e.g., Fig. A1 in Ref. [58]). For all cases of Table I, the kurtosis of the velocity field is very close to $K = 3$, which is the value for a Gaussian distribution. The correlation length of the velocity field l_u, also given in Table I, is about half of the periodic domain size $L = 2\pi$, as can also be seen from Fig. 4. It decreases slightly as Re increases and is slightly larger in the saturated stage than in the kinematic stage for all Re_M. The velocity field thus becomes more volume filling as the magnetic field saturates. This is directly attributable to the dynamical effects of the magnetic fields.

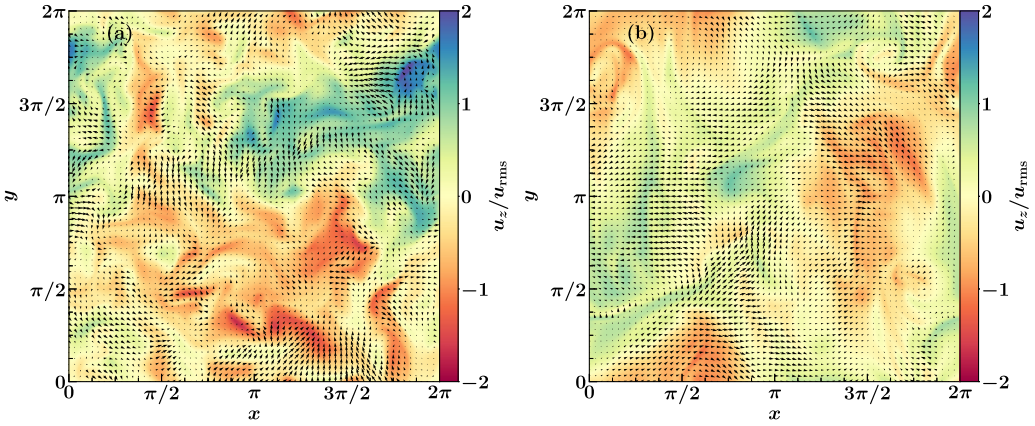

FIG. 4. A 2D cut in the xy plane with vectors $(u_x/\,u_{\rm rms}, u_y/\,u_{\rm rms})$ and color showing the magnitude of $u_z/\,u_{\rm rms}$ in the kinematic (a) and saturated (b) stages with $\mathrm{Re}_M = 2244$. The velocity field in both the stages looks qualitatively the same. The structures span approximately half of the domain.

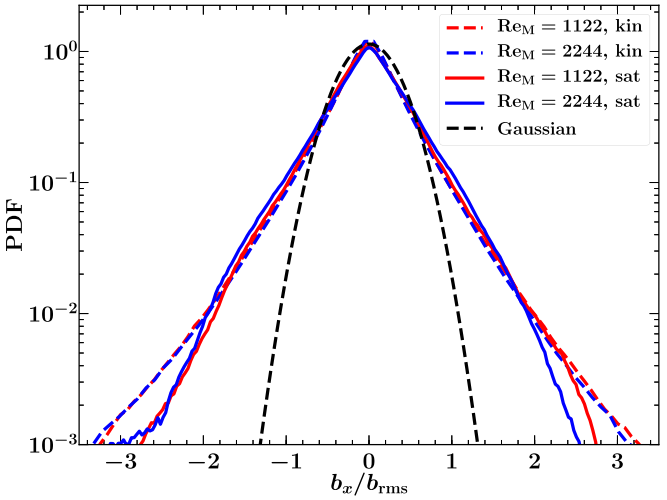

FIG. 5. The PDF of the normalized magnetic field component $b_x/\,b_{\rm rms}$ for $\mathrm{Re}_M = 1122$ and $\mathrm{Re}_M = 2244$ in the kinematic (dashed) and saturated (solid) stages for the values of Re_M given in the legend. The magnetic field for both Re_M in both stages is far from a Gaussian (dashed, black). It has heavy tails, which is a sign of intermittency. Here only $b_x/\,b_{\rm rms}$ is shown but similar behavior can be observed in all three magnetic field components.

Even though the velocity field statistics are nearly Gaussian, the magnetic field in both the kinematic and saturated stages is spatially intermittent and strongly non-Gaussian. This can be seen from the PDFs of a normalized component of the magnetic field $b_x/\,b_{\rm rms}$ in Fig. 5. The distribution is far from a Gaussian one and has long, heavy tails. The nonlinearity truncates the most extreme relative magnetic field strengths above $|b_x|/\,b_{\rm rms} \approx 3$. The magnetic field intermittency is further demonstrated in Fig. 6 which shows the PDF of $b/\,b_{\rm rms}$ for $\mathrm{Re}_M = 1122$ and $\mathrm{Re}_M = 2244$

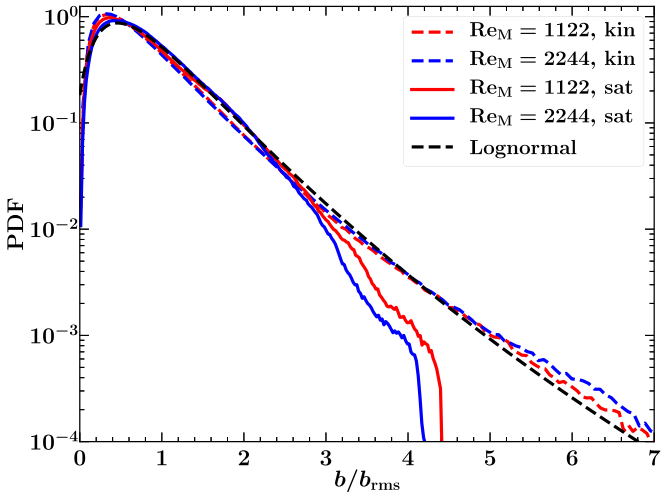

FIG. 6. The PDF of the normalized magnetic field strength $b/\,b_{\rm rms}$ for $\mathrm{Re}_M = 1122$ and $\mathrm{Re}_M = 2244$ in the kinematic (dashed) and saturated (solid) stages for the values of Re_M given in the legend. The PDF of the magnetic field in the kinematic state follows a lognormal distribution (dashed, black). The magnetic field is more intermittent in the kinematic stage than in the saturated stage.

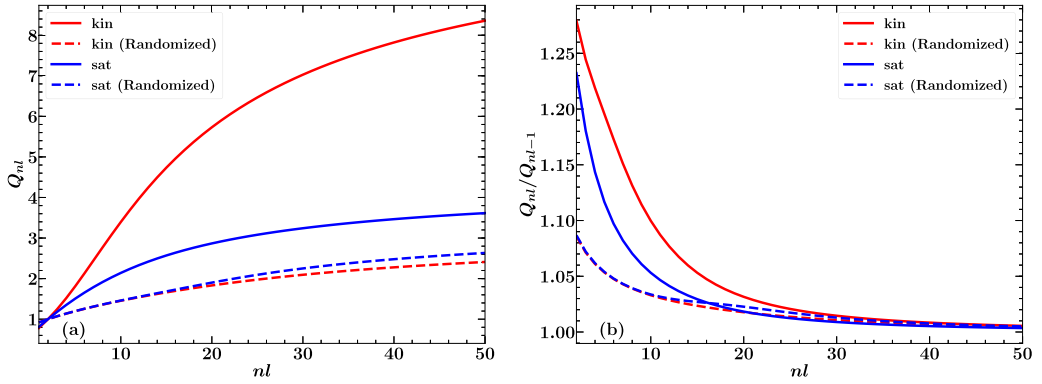

FIG. 7. $Q_{nl} = \langle (b/b_{\rm rms})^{nl} \rangle^{(1/nl)}$ (a) and Q_{nl}/Q_{nl-1} (b) as function of nl for the kinematic (red, solid) and saturated (blue, solid) stages for $\mathrm{Re}_M = 1122$. The corresponding quantities for randomized fields which have almost Gaussian statistics (dashed) are also plotted. The dynamo generated magnetic field is always intermittent with the degree of intermittency being higher in the kinematic stage.

in the kinematic and saturated stages. The PDF of the kinematic magnetic field strength follows a lognormal distribution and it has heavier tails in comparison to that of the saturated magnetic field. Thus, the magnetic field is intermittent in both the kinematic and the saturated stages, but the level of intermittency decreases as the field saturates. It should be noted that this conclusion is consistent with that of Schekochihin *et al.* [33] (Fig. 6 in this paper is similar to their Fig. 27), who studied a closely related system. This confirms that this finding is robust to small variations in the model setup and parameters.

Magnetic intermittency can also be quantified by measuring the quantity $Q_{nl} = \langle (b/b_{\rm rms})^{nl} \rangle^{(1/nl)}$ and its rate of change as nl changes (for example, Q_{nl}/Q_{nl-1}). Higher Q_{nl} and Q_{nl}/Q_{nl-1} is a signature of a larger degree of intermittency. Figure 7 shows Q_{nl} and Q_{nl}/Q_{nl-1} for the magnetic field in the kinematic and saturated stages for $\mathrm{Re}_M = 1122$ for $nl = 1, 2, 3, \ldots, 50$. Q_{nl} and its rate of change are higher for the kinematic stage as compared to the saturated stage. This further demonstrates that the magnetic field in the saturated stage is less intermittent than that in the kinematic stage. We further compare both terms with the corresponding Gaussian versions obtained by randomizing phases in Fourier space (keeping the exact same magnetic field spectrum but destroying intermittent structures, as done in Refs. [35,36,59]). Q_{nl} and Q_{nl}/Q_{nl-1} are higher for the dynamo generated field in comparison to its randomized Gaussian versions in both the kinematic and saturated stages. Thus, the dynamo generated field is always spatially intermittent and the degree of intermittency decreases as the field saturates due to nonlinearity.

The two-dimensional vector plots of the magnetic fields in Fig. 8 also show larger structures in the saturated stage. This can be further seen in Fig. 9, which shows the isosurfaces of magnetic fields in the kinematic and saturated stages. The kurtosis of the kinematic magnetic field for $\mathrm{Re}_M = 1122$ is 5.29 but is 3.32 in the saturated stage. This also suggests that the magnetic field in the kinematic stage is more intermittent than the saturated stage. The magnetic field correlation length l_b is calculated using Eq. (8) by replacing E_k with M_k, the magnetic field power spectrum. The magnetic field correlation length in the kinematic $l_{b\mathrm{kin}}$ and saturated $l_{b\mathrm{sat}}$ stages is given in Table I. The magnetic field correlation length decreases as Re_M increases, both for the kinematic and saturated stages (see Sec. V for further details). Thus, the magnetic field intermittency increases during both kinematic and saturated dynamo stages as Re_M increases. It is also clear that $l_{b\mathrm{sat}} > l_{b\mathrm{kin}}$ for all Re_M which confirms again that the magnetic field in the kinematic stage is less volume filling. The increase in the correlation length due to magnetic field saturation is true regardless of the choice of Re_M and agrees with previous numerical studies [26,40].

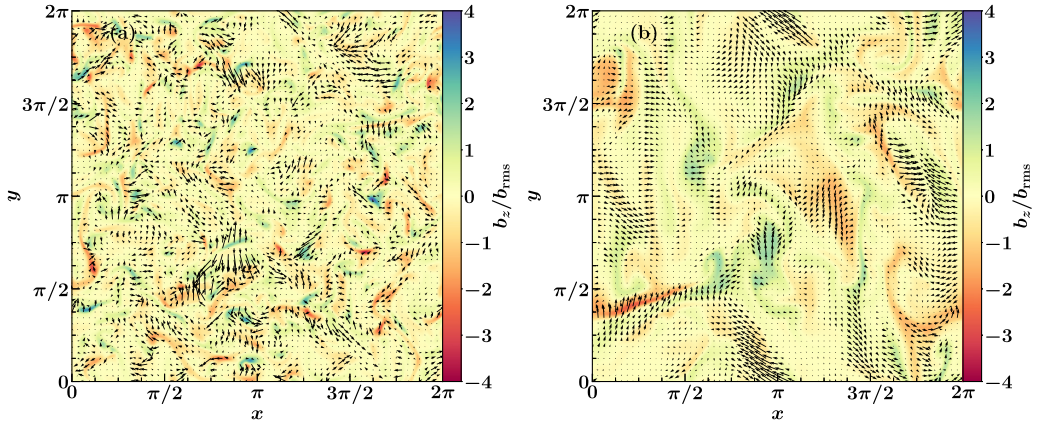

FIG. 8. As described in the caption of Fig. 4 but for the magnetic field. The magnetic field in the kinematic stage (a) is intermittent with random magnetic structures. In the saturated stage (b), the field remains intermittent but the structures are larger.

IV. SATURATION OF THE FLUCTUATION DYNAMO

Several mechanisms have previously been considered to explain the saturation of the fluctuation dynamo, including a reduction in magnetic field line stretching due to the suppression of the Lagrangian chaos in the velocity field [60,61], changes in the mutual alignment of the velocity and magnetic field lines [43], the folded structure of magnetic fields and energy equipartition between magnetic and velocity fields for $\mathrm{Pr}_M \gg 1$ [33,62], enhancement in diffusion due to additional nonlinear velocity drift [63,64] and selective dissipation of the turbulent kinetic energy [65,66]. From the induction Eq. (2), there are two type of processes that could lead to the saturation: a decrease in the induction term $[\boldsymbol{\nabla} \times (\mathbf{u} \times \mathbf{b})]$ or an increase in the dissipation term $(\eta \nabla^2 \mathbf{b})$. We explore each scenario here.

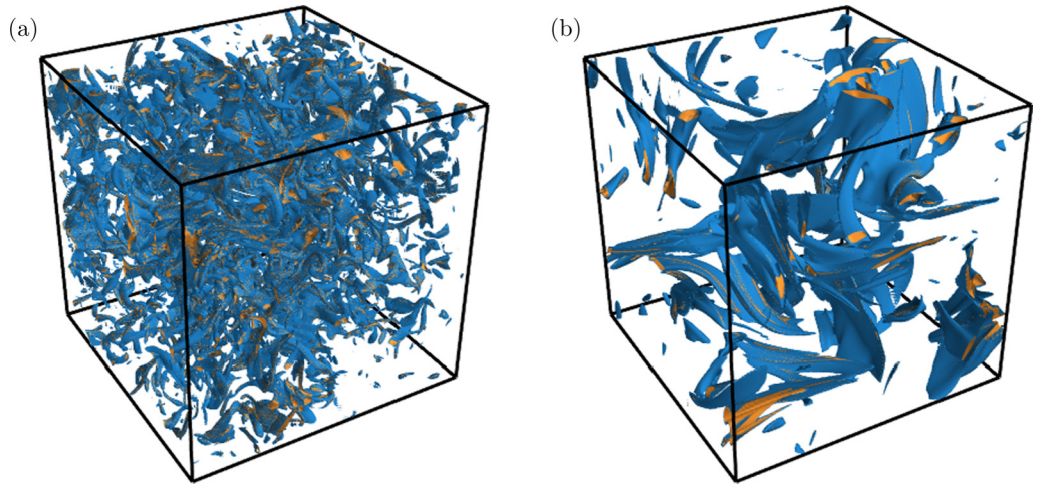

FIG. 9. Isosurfaces of $b^2/\,b^2_{\rm rms} = 4$ (blue) and $b^2/\,b^2_{\rm rms} = 5$ (yellow) for the magnetic fields in the kinematic (a) and saturated stages (b) for $\mathrm{Re}_M = 2244$. The structures in the saturated stage are larger in size as compared to that in the kinematic stage.

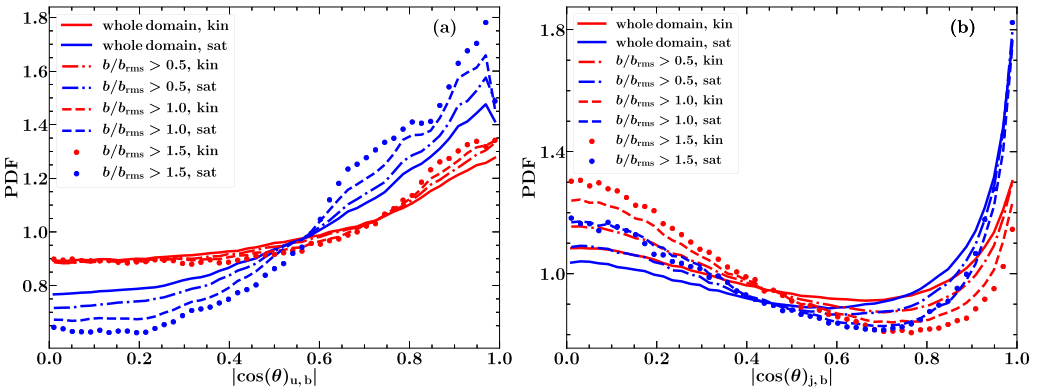

FIG. 10. The total and conditional probability distribution functions of the cosines of the angles between $\mathbf{u}$ and $\mathbf{b}$, $\cos(\theta)_{\mathbf{u},\,\mathbf{b}}$ (a) and between $\mathbf{j}$ and $\mathbf{b}$, $\cos(\theta)_{\mathbf{j},\,\mathbf{b}}$ (b) for $\mathrm{Re}_M = 1122$ in the kinematic (red) and saturated (blue) states. The magnetic field in the saturated stage is more aligned with the velocity field (reducing the induction effects) as compared to the kinematic stage. The magnetic field also becomes better aligned with the electric current density, reducing the back reaction on the velocity field.

A. Alignment of velocity field, magnetic field, and electric current density

We first examine how the induction term is affected when the field becomes stronger. The rms magnitude of both the velocity and magnetic fields are statistically steady, as shown in Fig. 1. Thus, we consider the alignment of the magnetic field with the velocity field as a possible mechanism for the saturation. Such an alignment has been studied in the context of convectively driven fluctuation dynamos [43,67], MHD turbulence in the presence of a strong guide field [68] and decaying isotropic MHD turbulence [69]. For the numerical simulations described in Table I, we calculate the angle between the velocity $\mathbf{u}$ and magnetic field $\mathbf{b}$, and between the current density $\mathbf{j}$ and $\mathbf{b}$,

$$\cos(\theta)_{\mathbf{u},\,\mathbf{b}} = \frac{\mathbf{u}\cdot\mathbf{b}}{|\mathbf{u}||\mathbf{b}|}, \quad \text{and} \quad \cos(\theta)_{\mathbf{j},\,\mathbf{b}} = \frac{\mathbf{j}\cdot\mathbf{b}}{|\mathbf{j}||\mathbf{b}|}, \tag{9}$$

respectively. An increase in the level of alignment between $\mathbf{u}$ and $\mathbf{b}$ implies a decrease in the effectiveness of magnetic induction; an increase in the level of alignment between $\mathbf{j}$ and $\mathbf{b}$ leads to a decrease in the Lorentz force, i.e., the field becomes more force-free.

Figures 10 and 11 show the probability density functions of the cosines in the kinematic and saturated stages for $\mathrm{Re}_M = 1122$ and $\mathrm{Re}_M = 1496$. Since both angles are symmetric about $\mathbf{b} = \mathbf{0}$,

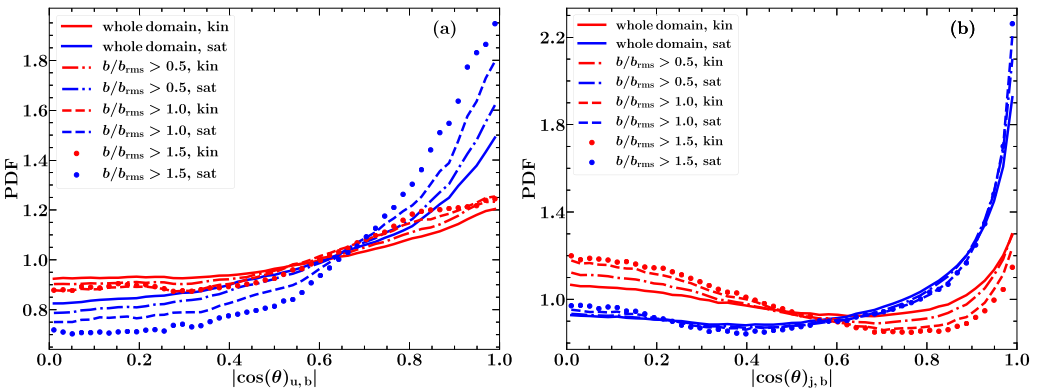

FIG. 11. As described in the caption of Fig. 10 but for $\mathrm{Re}_M = 1496$.

we show PDFs of the absolute value of their cosines. For both values of Re_M, the cosine of the angle between the velocity and magnetic field, $|\cos(\theta)_{\mathbf{u},\mathbf{b}}|$, tends to be larger in the saturated stage than in the kinematic stage. The better alignment between $\mathbf{u}$ and $\mathbf{b}$ decreases the induction term $\boldsymbol{\nabla} \times (\mathbf{u} \times \mathbf{b})$ and thus reduces the amplification of the magnetic field. To put this another way, the enhanced alignment between $\mathbf{u}$ and $\mathbf{b}$ implies a decrease in the energy transfer from the flow to the magnetic field (which is a process that has been studied in some detail in the context of shell models of magnetohydrodynamic turbulence [70–73]). However, there is a significant fraction of the volume where the two fields are not aligned and so the amplification is not completely suppressed. This minimum level of amplification is required to balance the magnetic diffusion. The cosine of the angle between the current density and magnetic field $\cos(\theta)_{\mathbf{j},\mathbf{b}}$ is also statistically larger by magnitude in the saturated stage. Thus, the field becomes closer to a force-free form as it saturates. This also implies that the morphology of magnetic field changes on saturation, which motivates us to study the morphology of magnetic structures in Sec. V. Overall, because of the enhanced local alignment between the velocity and magnetic field, the field amplification rate decreases. At the same time, due to the increase in the local alignment between the current density and magnetic field, the field becomes more force-free.

Similar broad conclusions apply when we consider conditional PDFs that focus exclusively upon the regions of stronger field (higher b/b_{rms} in Figs. 10 and 11). However, the level of alignment between the velocity and magnetic field is higher in the strong field regions in both the kinematic and saturated stages. This suggests that the strong field regions require a larger reduction in amplification by alignment. The distribution of $\cos(\theta)_{\mathbf{j},\mathbf{b}}$ in the kinematic stage shows some dependence upon the field strength but in the saturated stage the difference is less pronounced. In the kinematic stage, alignment is weakest in the relatively strong field regions, suggesting that in the strong field regions, not only because of its higher strength (as the Lorentz force is proportional to the strength of the field) but also because of the lower level of alignment, the field produces a stronger back reaction on the flow.

Another important question is whether the alignment between the velocity and magnetic fields and the magnetic field and current density occur in the same spatial region. To answer this, we show the cross-correlation between the two angles in Fig. 12, which suggests that the velocity, magnetic field, and current density are always nearly aligned to each other at same spatial positions. It is difficult to see any further difference between the kinematic and saturated stages in Figs. 12(a) and 12(b). Figures 12(c) and 12(d) show the same correlation but only for strong field regions, $b/b_{\mathrm{rms}} > 1.5$. In Fig. 12(c), the kinematic stage shows higher correlation in regions with high $\cos(\theta)_{\mathbf{u},\mathbf{b}}$ and low $\cos(\theta)_{\mathbf{j},\mathbf{b}}$, which is absent in the saturated stage. The larger misalignment of $\mathbf{j}$ and $\mathbf{b}$, especially in the strong field regions, enhances the work done on the magnetic field by the flow. This promotes growth of the magnetic field. Once the field saturates, the larger correlation at high $\cos(\theta)_{\mathbf{u},\mathbf{b}}$ and low $\cos(\theta)_{\mathbf{j},\mathbf{b}}$ disappears in Fig. 12(d). This implies a statistical decrease in the back-reaction of the magnetic field on the flow as the field saturates.

To summarize, the alignment between the velocity and magnetic field vectors and the magnetic field and current density vectors is statistically enhanced as the dynamo saturates. The alignment does not completely inhibit the amplification, so there is always some field generated to balance the resistive decay. This in turn also implies that the back reaction of the Lorentz force always remains significant.

B. Magnetic field stretching

To explore another mechanism by which magnetic field amplification can be suppressed, we consider the stretching of the magnetic field lines by the turbulent velocity. For this, we consider the alignment of the magnetic field with the eigenvectors of the rate of strain tensor. Neglecting the rather weak divergence of the flow, the symmetric 3×3 matrix $S_{ij} = \frac{1}{2}(u_{i,j} + u_{j,i})$ is calculated at each point in the domain using sixth-order finite differences, and its eigenvalues and eigenvectors are calculated. The eigenvalues are arranged in an increasing order, $\lambda_1 < \lambda_2 < \lambda_3$. The corresponding

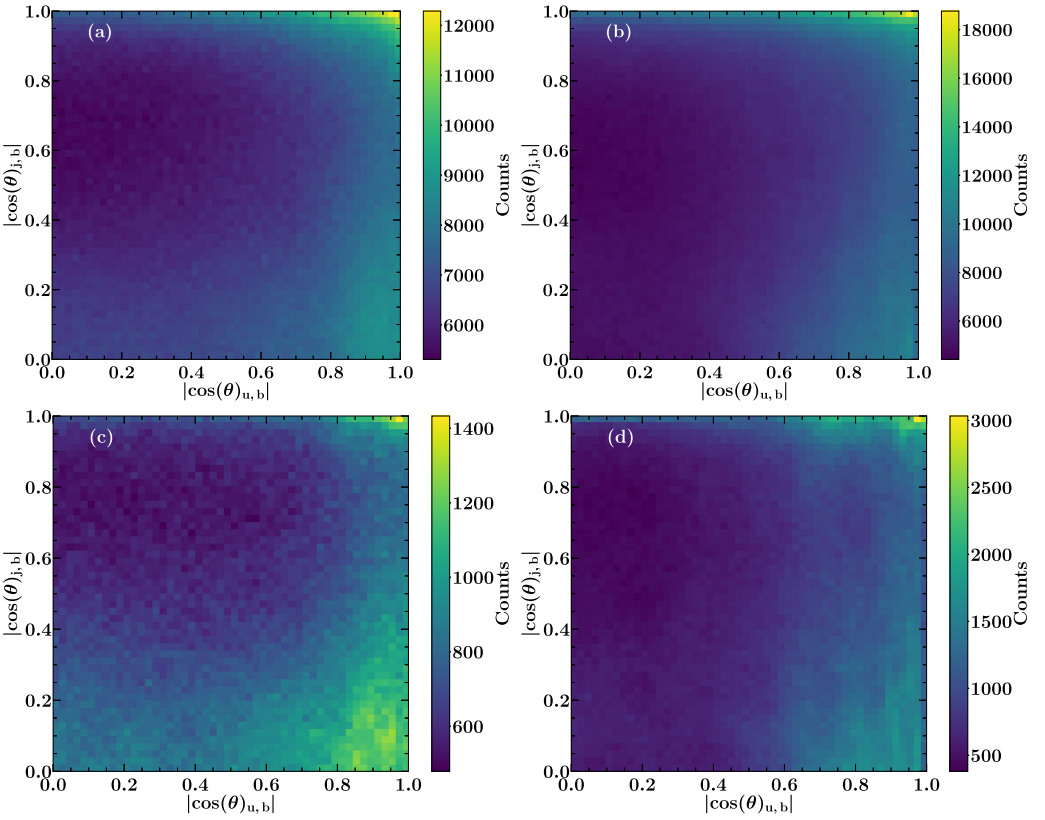

FIG. 12. The cross correlation of $\cos(\theta)_{\mathbf{u},\,\mathbf{b}}$ and $\cos(\theta)_{\mathbf{j},\,\mathbf{b}}$ in the kinematic (a, c) and saturated (b, d) stages for $\mathrm{Re}_M = 1122$. Panels (a) and (b) refer to the whole domain and the difference between them is not significant. Panels (c) and (d) refers to only the strong field regions ($b/\,b_{\mathrm{rms}} \geqslant 1.5$). The yellow patch close to low $\cos(\theta)_{\mathbf{j},\,\mathbf{b}}$ and high $\cos(\theta)_{\mathbf{u},\,\mathbf{b}}$ in the kinematic stage vanishes for the saturated stage. The peak in the count is always at high $\cos(\theta)_{\mathbf{u},\,\mathbf{b}}$ and high $\cos(\theta)_{\mathbf{j},\,\mathbf{b}}$, which implies significant alignment between magnetic field, velocity field and current density.

eigenvectors are $\mathbf{e}_1, \mathbf{e}_2, \mathbf{e}_3$. The sum of the eigenvalues is close to zero since the flow is nearly incompressible. λ_1 is always negative and the vector $\mathbf{e}_1$ corresponds to the direction of local compression of magnetic field, λ_3 is always positive and the vector $\mathbf{e}_3$ corresponds to the direction of local stretching, whereas λ_2 can be obtained from $\lambda_1 + \lambda_2 + \lambda_3 \approx 0$. The direction $\mathbf{e}_2$ (sometimes referred to as the "null" direction [33,74]) can correspond to either local stretching or compression depending on the sign of λ_2. We then quantify the alignment with the magnetic field $\mathbf{b}$ of the vectors $\mathbf{e}_1$ and $\mathbf{e}_3$ by considering

$$\cos(\theta)_{\mathbf{e}_1,\,\mathbf{b}} = \frac{\mathbf{e}_1 \cdot \mathbf{b}}{|\mathbf{e}_1||\mathbf{b}|} \quad \text{and} \quad \cos(\theta)_{\mathbf{e}_3,\,\mathbf{b}} = \frac{\mathbf{e}_3 \cdot \mathbf{b}}{|\mathbf{e}_3||\mathbf{b}|}. \tag{10}$$

Figure 13 shows the PDF of the cosines in the kinematic and saturated stages for $\mathrm{Re}_M = 1796$. In most of the volume, the direction of the magnetic field is perpendicular to the direction of the local compression [Fig. 13(a)], which leads to the amplification of magnetic field, and this trend is slightly stronger in the kinematic stage. The PDF of the angle between the direction of local stretching and the magnetic field $\cos(\theta)_{\mathbf{e}_3,\,\mathbf{b}}$ has maxima at $\cos(\theta)_{\mathbf{e}_3,\,\mathbf{b}} = 0$ and $\cos(\theta)_{\mathbf{e}_3,\,\mathbf{b}} = 1$ in the kinematic stage. In the saturated stage, however, all angles are nearly equiprobable. This change in

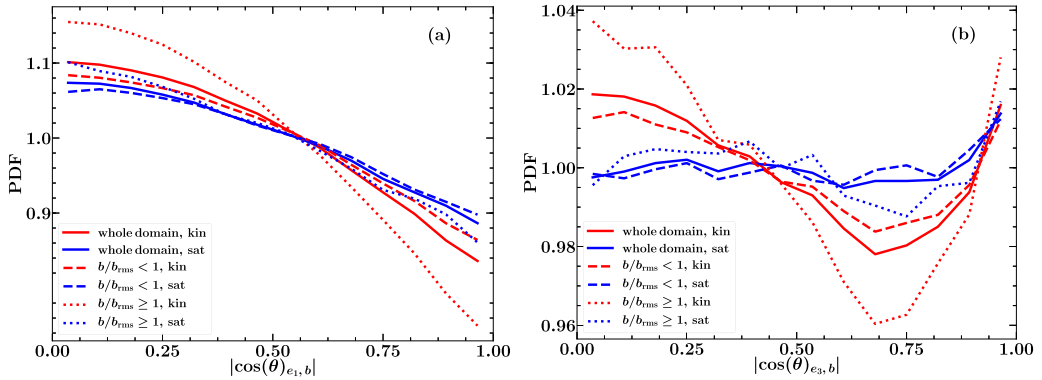

FIG. 13. The total and conditional PDFs of the cosine of the angle between the direction of local field line compression and the magnetic field $\cos(\theta)_{\mathbf{e}_1,\mathbf{b}}$ (a) and between the direction of local field line stretching and the magnetic field $\cos(\theta)_{\mathbf{e}_3,\mathbf{b}}$ (b) for $\mathrm{Re}_M = 1796$ in the kinematic (red) and saturated (blue) stages.

behavior is more pronounced in the strong field regions, $b/\,b_{\rm rms} \geqslant 1$. In Fig. 14(a), we also show the PDF of $\cos(\theta)_{\mathbf{e}_2,\mathbf{b}}$, $\cos(\theta)_{\mathbf{e}_1,\mathbf{b}}$, and $\cos(\theta)_{\mathbf{e}_3,\mathbf{b}}$. The forms of the PDF for $\cos(\theta)_{\mathbf{e}_2,\mathbf{b}}$ are different from that of $\cos(\theta)_{\mathbf{e}_1,\mathbf{b}}$ and $\cos(\theta)_{\mathbf{e}_3,\mathbf{b}}$ in the kinematic and saturated stages. The magnetic field is less aligned to the direction $\mathbf{e}_2$ in the kinematic stage as compared to the saturated stage and its effect, locally on the magnetic field, is decided by the sign of the eigenvalue λ_2 [dashed lines in Fig. 14(b)]. Figure 14(b) shows the PDF of all three eigenvalues in the kinematic and saturated stages. All three eigenvalues are statistically lower in magnitude in the saturated stage as compared to the kinematic stage. However, as can be seen in Figs. 13 and 14(a), the difference between the PDFs in the kinematic and saturated stages, while statistically significant, is not very strong. This suggest that a small reduction in the local stretching and compression of magnetic field contributes toward the saturation of the fluctuation dynamo.

Before concluding this section, we note that some of these conclusions are similar to those reached independently in the PhD thesis of Denis St-Onge [74], albeit for a different model setup.

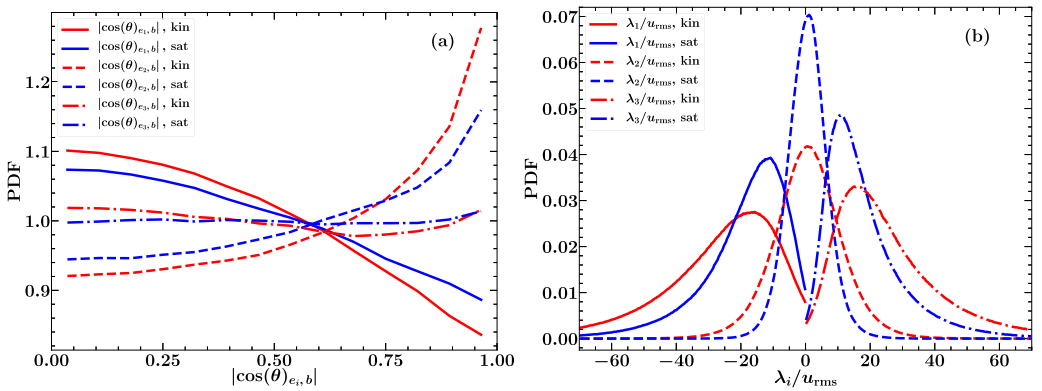

FIG. 14. The PDFs of the cosine of the angle between three three eigenvectors ($\mathbf{e}_1$, $\mathbf{e}_2$, and $\mathbf{e}_3$) with the local magnetic field direction (a) and three three eigenvalues (λ_1, λ_2, and λ_3) normalized by $u_{\rm rms}$ (b) for $\mathrm{Re}_M = 1796$ in the kinematic (red) and saturated (blue) stages.

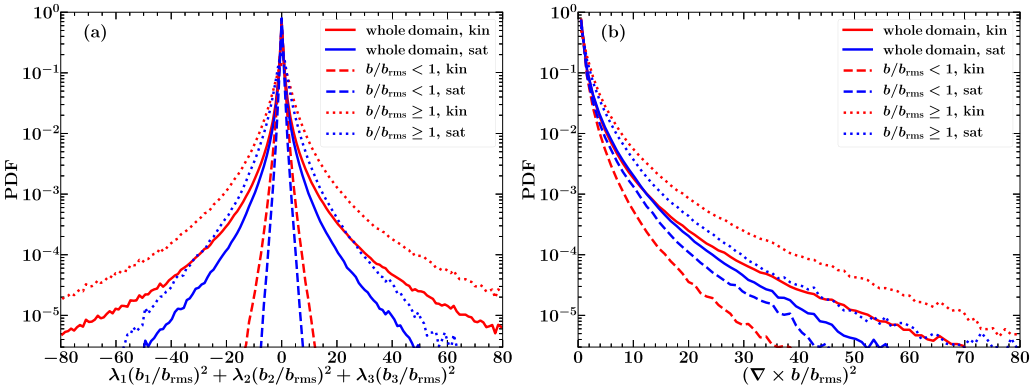

FIG. 15. The total and conditional PDFs of the local growth term $\lambda_1(\mathbf{b}_1/b_{\rm rms})^2 + \lambda_2(\mathbf{b}_2/b_{\rm rms})^2 + \lambda_3(\mathbf{b}_3/b_{\rm rms})^2$ (a) and the local dissipation term $(\nabla \times \mathbf{b})^2$ (b) in the kinematic (red) and saturated (blue) stages for $\mathrm{Re}_M = 1122$. The skewness of the local growth term distribution (solid red line in (a)) is 0.4 in the kinematic stage and 0.1 in the saturated stage (solid blue line), so the tendency of this term to promote growth decreases on saturation, as could be expected. The local dissipation term (b) also decreases statistically as the field saturates. This conclusions hold in both the weak and strong field regions, except for the local dissipation term, which increases in the weak field regions.

C. Local magnetic energy balance

We now directly consider the equation for magnetic energy evolution and calculate its local growth and dissipation terms. For an incompressible flow in a periodic domain, the magnetic energy evolution equation can be written as [75]

$$\frac{dE_M}{dt} = \int_V b_i b_j S_{ij}\, dV - \eta \int_V (\nabla \times \mathbf{b})^2\, dV, \tag{11}$$

where $E_M = \frac{1}{2}\int_V \mathbf{b}^2\, dV$ and summation over repeated indices is understood. The term contributing to the energy growth, $b_i b_j S_{ij}$, is calculated at each point in the volume as follows. First, we project the magnetic field vector $\mathbf{b}$ on to each of the eigenvectors of the rate of strain tensor, $\mathbf{e}_1, \mathbf{e}_2, \mathbf{e}_3$. Let these be $\mathbf{b}_1, \mathbf{b}_2, \mathbf{b}_3$, and then the local growth term $b_i b_j S_{ij} = \lambda_1 \mathbf{b}_1^2 + \lambda_2 \mathbf{b}_2^2 + \lambda_3 \mathbf{b}_3^2$ at each position. This term can be positive or negative ($\lambda_1 < 0$ and $\lambda_3 > 0$). A negative local growth term leads to a decrease in the magnetic energy, while a positive value leads to an increase. The term contributing to the decay in energy is calculated by computing $(\nabla \times \mathbf{b})^2$ (η = constant) at each point in space.

Figures 15 and 16 show the total and conditional PDFs of the local growth and dissipation terms in the kinematic and saturated stages for $\mathrm{Re}_M = 1122$ and $\mathrm{Re}_M = 1796$, respectively. Figures 15(a) and 16(a) show that the local growth term decreases on saturation and this is equally true of the strong and weak field regions. This confirms that the stretching of the magnetic field line reduces, which in turn decreases the amplification. Numerically, this can be quantified by calculating the skewness of the local growth term distribution in the kinematic and saturated stages [solid red and blue lines in Figs. 15(a) and 16(a)]. The skewness is defined for a quantity X as $\langle (X - \langle X \rangle)^3 \rangle / \langle (X - \langle X \rangle)^2 \rangle^{3/2}$, where $\langle \cdots \rangle$ refers to the mean. The skewness of the local growth term distribution in the kinematic [solid red line in Fig. 15(a)] and saturated [solid blue line in Fig. 15(a)] stage for $\mathrm{Re}_M = 1122$ are 0.4 and 0.1, respectively. The corresponding values for $\mathrm{Re}_M = 1796$ [Fig. 16(a)] in the kinematic and saturated stages are 0.9 and 0.4, respectively. The local growth term always has a positive skewness implying continuous magnetic field generation. The skewness decreases on saturation, where the growth is only required to compensate the dissipation. The dissipation term also exhibits an overall decrease on saturation as shown in Figs. 15(b) and 16(b), but its behavior differs in the strong and weak field regions, where the dissipation increases in the latter regions.

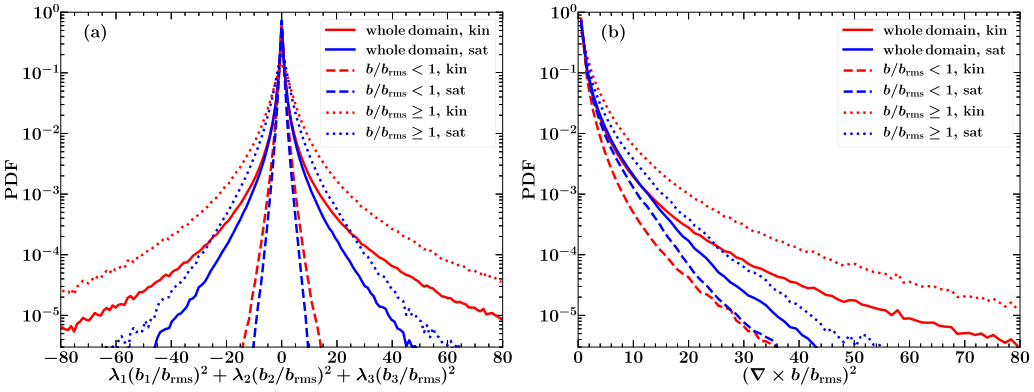

FIG. 16. As Fig. 15 but for $\mathrm{Re}_M = 1796$. The skewness of the local growth term distribution [solid red line in (a)] is 0.9 in the kinematic stage and 0.4 in the saturated stage (solid blue line). The conclusions remain the same here as for $\mathrm{Re}_M = 1122$ in Fig. 15.

To calculate the overall decrease or increase in the magnetic energy at each point in the domain, we calculate the local magnetic Reynolds number. This helps us to explore the behavior of the diffusion term ($\eta\nabla^2\mathbf{b}$) in the induction equation [Eq. (2)] as the dynamo saturates. Both terms in Eq. (11) are calculated at each point in the volume, and the local magnetic Reynolds number is derived at each position as

$$(\mathrm{Re}_M)_{\rm loc} = \frac{b_i b_j S_{ij}}{\eta(\nabla \times \mathbf{b})^2}, \tag{12}$$

providing a measure of the local dynamo efficiency. The local magnetic Reynolds number can be positive or negative, signifying the locally increasing or decreasing magnetic field strength, respectively. Figures 17 and 18 show the total and conditional PDFs of the local magnetic Reynolds number in the kinematic and saturated stages for $\mathrm{Re}_M = 1122$ and $\mathrm{Re}_M = 1796$. $(\mathrm{Re}_M)_{\rm loc}$ varies from values much less than to those much greater than $\mathrm{Re}_M^{(\rm crit)}$ in both the kinematic and saturated stages. Thus, magnetic field grows and decays in different parts of the volume but remains in a

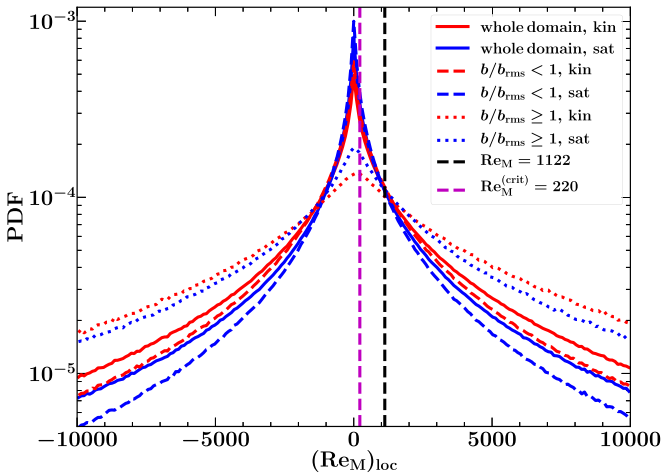

FIG. 17. The total and conditional PDFs of the local magnetic Reynolds number $(\mathrm{Re}_M)_{\rm loc}$ in the kinematic (red) and saturated (blue) stages with $\mathrm{Re}_M = 1122$. The purple dashed line shows the critical magnetic Reynolds number $\mathrm{Re}_M^{(\rm crit)} = 220$ and the black dashed line shows Re_M for this run.

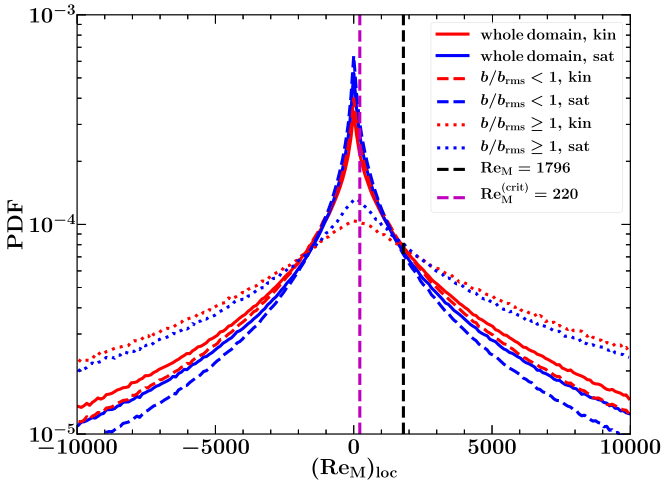

FIG. 18. As described in the caption of Fig. 17 but for $\mathrm{Re}_M = 1796$.

statistically steady state overall in the saturated stage. On saturation, both Figs. 17 and 18 show that $(\mathrm{Re}_M)_{\mathrm{loc}}$ decreases statistically. The mean of $(\mathrm{Re}_M)_{\mathrm{loc}}$ for $\mathrm{Re}_M = 1122$ in the kinematic stage is 808 and that in the saturated stage is 595. Thus, the mean value of the local magnetic Reynolds number over the entire domain decreases on saturation (to a value close to but not exactly equal to the critical value, $\mathrm{Re}_M^{(\mathrm{crit})} \approx 220$). This effectively implies a relative enhancement in the local diffusion in comparison to the local stretching, which also contributes toward the saturation of the fluctuation dynamo.

To summarize, the fluctuation dynamo saturates due to both reduction in stretching and altered diffusion. The alignment between the velocity and magnetic fields increases as the field saturates, signifying reduced amplification. Furthermore, the current density and magnetic field are also statistically better aligned in the saturated stage, which implies a trend toward a force-free field. The local growth term statistically decreases (the skewness of the distribution, though remaining positive, decreases on saturation), which implies that the reduced magnetic field stretching reduces the amplification, which contributes toward the saturation of the fluctuation dynamo. The local magnetic Reynolds number, though varying over a wide range from values much less than to much higher than the critical value, decreases on average. This further implies relative enhancement in the local dissipation compared to the local stretching, which also contributes toward the saturation of the fluctuation dynamo.

V. MORPHOLOGY OF MAGNETIC STRUCTURES

As shown in Sec. III, magnetic field generated by a fluctuation dynamo is intermittent as it is concentrated in filaments, sheets and ribbons (Figs. 8 and 9). To characterize the magnetic structures, we use the Minkowski functionals [76]. Minkowski functionals have been used in studying morphology of structures in a number of numerical simulations [34,77–82] and observations [83–86]. The morphology of a d-dimensional structure can be described by $d + 1$ Minkowski functionals. In three dimensions, there are four Minkowski functionals, as described in Table II. We calculate the Minkowski functionals using Crofton's formulas [87,88] and then calculate the representative length scales (l_1, l_2, l_3) of magnetic structures (defined by isosurfaces at a fixed value of the magnetic field strength, e.g., see Fig. 9) as [77,89]

$$l_1 = \frac{V_0}{2V_1}, \quad l_2 = \frac{2V_1}{\pi V_2}, \quad l_3 = \frac{3V_2}{4V_3}. \tag{13}$$

TABLE II. Four Minkowski functionals (MF) V_0, V_1, V_2, and V_3, their geometrical interpretation and definitions in three dimensions. dV is the volume element, dS is the surface element, and κ_1 and κ_2 are the principle curvatures of the surface of a structure.

MF	Geometric interpretation	Expression
V_0	Volume	$\iiint dV$
V_1	Surface area	$(1/6)\iint dS$
V_2	Integral mean curvature	$(1/6\pi)\iint(\kappa_1+\kappa_2)\,dS$
V_3	Euler characteristic	$(1/4\pi)\iint(\kappa_1\kappa_2)\,dS$

We associate the smallest of these length scales with the thickness T of the structures, the next largest with the width W, and the largest length scale with the length L, i.e., if $l_1 \leqslant l_2 \leqslant l_3$, then $T = l_1, W = l_2,$ and $L = l_3$. The thickness, width, and length can be further used to obtain dimensionless measures of the structure shape: planarity p and filamentarity f, given by

$$p = \frac{W-T}{W+T}, \quad f = \frac{L-W}{L+W}. \tag{14}$$

By definition, $0 \leqslant p \leqslant 1$ and $0 \leqslant f \leqslant 1$; $p = 0$ and $f = 1$ for a perfect filament, $p = 0$ and $f = 0$ for a sphere, and $p = 1$ and $f = 0$ for a sheet. The planarity and filamentarity are not sensitive to the size of the structures but quantify the shape. It is useful to remember that, unlike the Minkowski functionals, p and f are not additive.

To explore the morphology of magnetic structrures for a range of Re_M values, we use simulations with parameters given in Table III. We keep Re about the same for all runs, vary Re_M (making sure $\mathrm{Pr}_M \geqslant 1$), and choose $k_\mathrm{F} \approx 5(2\pi/L)$, so there is a sufficient number of magnetic correlation cells within the volume (with 5^3 velocity correlation cells).

Figure 19(a) shows the thickness, width, and length of magnetic structures obtained by averaging over 30 values of magnetic field strengths ranging from $b/\,b_\mathrm{rms} = 2.5$ to 4. The lower limit of the magnetic field strength is chosen to ensure that the structures represent the tail of the PDF (e.g., see Fig. 6), while the upper limit is chosen to ensure a sufficient number of points within each structure. The computed values of planarity and filamentarity also remain roughly constant within this selected range of magnetic field strengths. For the kinematic stage, we expect that the largest length scale L will be independent of Re_M. This is because the length of the structures is controlled by the correlation length of the flow since the magnetic correlation function of the fastest

TABLE III. Parameters of various runs for the nonlinear fluctuation dynamo in a numerical domain size of $(2\pi)^3$ with 512^3 mesh points. In all cases, the forcing scale is approximately $L/5$, the forcing amplitude is $F_0 \approx 0.02$ and the hydrodynamic viscosity is $\nu = 4\times10^{-4}$. The magnetic diffusivity η, the rms velocity in the saturated stage u_rms, the Reynolds number Re, the magnetic Reynolds number Re_M, the magnetic Prandtl number Pr_M and the critical magnetic Reynolds number $\mathrm{Re}_M^{(\mathrm{crit})}(\approx 220\mathrm{Pr}_M^{-1/2})$ are given.

η	u_rms	Re	Re_M	Pr_M	$\mathrm{Re}_M^{(\mathrm{crit})}$
4×10^{-4}	0.11	346	346	1.00	220
3×10^{-4}	0.11	346	461	1.33	191
2×10^{-4}	0.10	314	628	2.00	156
1×10^{-4}	0.09	283	1131	4.00	110
7.5×10^{-5}	0.09	283	1508	5.33	95
5×10^{-5}	0.09	283	2261	8.00	78

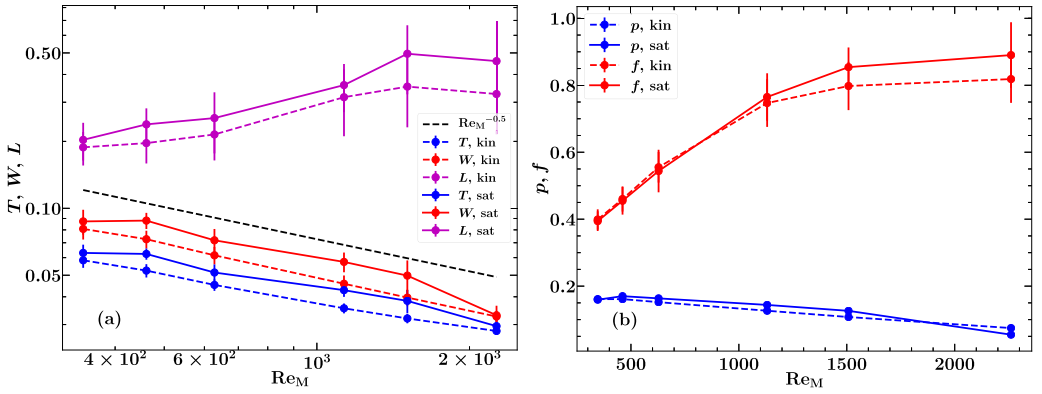

FIG. 19. (a) Average length (L), thickness (T) and width (W) of magnetic structures in the kinematic (dashed, color) and saturated stages (solid, color) of the nonlinear fluctuation dynamo as functions of Re_M. The width and thickness of the magnetic structures both decrease as $\mathrm{Re}_M^{-0.5}$. The Re_M dependence of the size of the structures is approximately the same in both the kinematic and saturated stages. (b) Planarity (p) and filamentarity (f) of the magnetic structures, as functions of Re_M, for the kinematic (dashed, color) and saturated (solid, color) stages. As Re_M increases, the filamentarity increases and the planarity decreases but they seem to approach an asymptotic value after $\mathrm{Re}_M \approx 1200$. The trend with respect to Re_M is the same for both the kinematic and saturated stages.

growing dynamo mode decreases exponentially after that scale [32]. As seen in Fig. 19(a), the length remains roughly constant but then increases slightly after $\mathrm{Re}_M \approx 600$ and again remains roughly constant. This variation is likely to be due to the decrease in the Reynolds number Re (Table III). The other two scales (W and T) decrease as $\mathrm{Re}_M^{-0.5}$. This scaling can be obtained by balancing the rate of magnetic dissipation with the local shearing rate [90], $\eta/W^2 \simeq u_{\mathrm{rms}}/l_0$, where η is the magnetic resistivity, u_{rms} is the rms turbulent velocity, and l_0 is the driving scale of the turbulence. This gives $W \simeq l_0(\eta/u_{\mathrm{rms}}l_0)^{1/2} = l_0\mathrm{Re}_M^{-0.5}$. This means that the shape of the magnetic structures becomes more filamentary ($L \gg W \approx T$) and ribbonlike ($T \lesssim W \ll L$) as Re_M increases, but the filamentarity is always larger than the planarity, so the filaments dominate among the magnetic structures [91]. The differences in Re_M scalings with the previous work [34] is probably due to the following reasons. First, they have a prescribed velocity field with forcing at a range of scales, whereas we force the flow at two scales ($k = 4$ and $k = 6$) and then let it evolve via the Navier-Stokes equation. Second, our simulations are at a higher resolution (512^3) as compared to theirs (128^3) and thus magnetic structures, especially at higher Re_M, are better resolved in our case. Last and most importantly, they consider values of Re_M which are both lower and higher than $\mathrm{Re}_M^{(\mathrm{crit})}$, whereas we only consider $\mathrm{Re}_M > \mathrm{Re}_M^{(\mathrm{crit})}$. This is because we strongly believe that those two regimes ($\mathrm{Re}_M < \mathrm{Re}_M^{(\mathrm{crit})}$ and $\mathrm{Re}_M \geqslant \mathrm{Re}_M^{(\mathrm{crit})}$) are physically different and must not be considered together to characterize the length scales of magnetic structures as functions of Re_M.

All three scales are larger in the saturated stage than in the kinematic stage. Thus, the magnetic structures become larger as the magnetic field saturates. This is also the reason that the magnetic field correlation length scale increases as the field saturates (as shown in Table I). The increase in the length (the largest length scale) of magnetic structures on saturation is consistent with the finding by Schekochihin *et al.* [33]. The Re_M scaling for all three scales is roughly the same for both the kinematic and saturated stages.

Figure 19(b) shows the planarity and filamentarity of magnetic structures as functions of Re_M. The filamentarity is always higher than the planarity and thus the magnetic structures are more like filaments in both the kinematic and saturated stages. The dependence of these morphological measures on Re_M is the same for the kinematic and saturated stages.

VI. CONCLUSIONS AND DISCUSSION

It is important to understand the saturated state of the fluctuation dynamo because the saturated state seeds the mean field dynamo, controls the small-scale magnetic field structure, and decides the magnetic field length scales in the system where the mean field dynamo is absent (for example, elliptical galaxies). Moreover, it is crucial to understand the physics of the saturation mechanism because numerical simulations, at present, are at much lower values of Re_M than their estimated values ($\mathrm{Re}_M \approx 10^{18}$ for spiral galaxies, $\mathrm{Re}_M \approx 10^{22}$ for elliptical galaxies, and $\mathrm{Re}_M \approx 10^{29}$ for galaxy clusters).

Using numerical simulations of driven nearly incompressible turbulence, we have explored the saturation mechanism of the fluctuation dynamo. We find that the dynamo saturates because both the amplification and diffusion are affected by the action of the Lorentz force on the flow. Most previously suggested mechanisms hinted at changes in either of those two and thus required significant changes in the properties of the velocity and magnetic fields from the kinematic stage. For example, if only the enhancement in diffusion is responsible, then it would require the effective Re_M in the saturated state to reduce from hugely supercritical levels to values close to $\mathrm{Re}_M^{(\mathrm{crit})}$ ($\simeq 10^2$–10^3 [14]). And, if only the decrease in amplification is responsible for saturating the dynamo, then it would require a drastic decrease in the Lyapunov exponents (which are a measure of chaotic properties of the flow) [60]. We suggest that both occur and thus such a dramatic change is not necessary. We confirm that the amplification decreases by reduction in the stretching of magnetic field lines. The local magnetic Reynolds number $(\mathrm{Re}_M)_{\mathrm{loc}}$, which is suggested as a measure of the local magnetic diffusion, decreases slightly. This confirms that the local diffusion of magnetic field relative to field line stretching is enhanced, which is also responsible for saturating the dynamo.

The fluctuation dynamo-generated magnetic field is spatially intermittent. So, we studied the morphology of the magnetic structures in the kinematic and saturated stages. In both cases, the largest length scale is roughly independent of Re_M and the other two scales decrease as $\mathrm{Re}_M^{-0.5}$. We find that the structures are of a larger size (all three length scales increase) in the saturated stage as compared to the kinematic stage. This agrees with the results in Table I, where we find that the correlation length is higher for the saturated magnetic field. This also aligns with the conclusion in the Sec. III (also shown in Ref. [33]) that the magnetic field is less intermittent in the saturated stage as compared to the kinematic stage. However, the Re_M dependence is the same for both the stages and thus the overall shape of magnetic structures produced by the fluctuation dynamo is not affected by the Lorentz force to any significant extent (all three length scales increase but in a very similar way).

The study explores physical effects over a range of Re_M for $\mathrm{Pr}_M \geqslant 1$. However, for $\mathrm{Pr}_M > 1$ at very high Re_M ($\gtrsim 10^3$), the fields might be unstable to fast magnetic reconnection [12]. This might change the morphology of magnetic fields, locally affect velocity fields and thus might alter the saturated state of the fluctuation dynamo. However, the effect of fast, stochastic magnetic reconnection on the dynamo is not very well understood yet [92] and would require high-resolution numerical simulations over a number of very high Re_M values to study the effect of fast magnetic reconnection on the fluctuation dynamo saturation mechanism.

The study can be extended in several ways. An immediate extension would be to repeat the entire analysis for dynamos in a stratified medium [42,46,47,93], which is more relevant for young galaxies and star-forming gas clouds. We have performed the analysis for $\mathrm{Pr}_M \geqslant 1$ which is of relevance to fluctuation dynamo in the interstellar and intergalactic medium but this should be extended to the $\mathrm{Pr}_M < 1$ regime which is important for stars, planets and liquid metal experiments [94,95]. We have adopted the MHD approximation but plasma effects might also play an important role. It would also be interesting to compare our results with those of the plasma dynamo [96,97] and see how the relationship between velocity and magnetic fields and the magnetic field structure change when plasma effects are considered. Plasma effects might be particularly important for the weakly collisional gas in galaxy clusters. We aim to consider such problems in our future work.

ACKNOWLEDGMENTS

We thank Kandaswamy Subramanian and Christoph Federrath for useful discussions and comments on the paper. We acknowledge financial support of the STFC (Grant No. ST/N000900/1, Project 2) and the Leverhulme Trust (Grant No. RPG-2014-427).

[1] B. M. Gaensler, M. Haverkorn, L. Staveley-Smith, J. M. Dickey, N. M. McClure-Griffiths, J. R. Dickel, and M. Wolleben, The magnetic field of the large magellanic cloud revealed through Faraday rotation, Science **307**, 1610 (2005).

[2] A. Fletcher, R. Beck, A. Shukurov, E. M. Berkhuijsen, and C. Horellou, Magnetic fields and spiral arms in the galaxy M51, Mon. Not. R. Astron. Soc. **412**, 2396 (2011).

[3] M. Houde, A. Fletcher, R. Beck, R. H. Hildebrand, J. E. Vaillancourt, and J. M. Stil, Characterizing magnetized turbulence in M51, Astrophys. J. **766**, 49 (2013).

[4] F. Govoni and L. Feretti, Magnetic fields in clusters of galaxies, Int. J. Mod. Phys. D **13**, 1549 (2004).

[5] A. A. Schekochihin and S. C. Cowley, Turbulence, magnetic fields, and plasma physics in clusters of galaxies, Phys. Plasmas **13**, 056501 (2006).

[6] R. Beck, Magnetic fields in spiral galaxies, Ann. Rev. Astron. Astrophys. **24**, 4 (2016).

[7] R. Beck, A. Brandenburg, D. Moss, A. Shukurov, and D. Sokoloff, Galactic magnetism: Recent developments and perspectives, Ann. Rev. Astron. Astrophys. **34**, 155 (1996).

[8] L. M. Widrow, Origin of galactic and extragalactic magnetic fields, Rev. Mod. Phys. **74**, 775 (2002).

[9] A. Brandenburg and K. Subramanian, Astrophysical magnetic fields and nonlinear dynamo theory, Phys. Rep. **417**, 1 (2005).

[10] R. M. Kulsrud and E. G. Zweibel, On the origin of cosmic magnetic fields, Rep. Prog. Phys. **71**, 046901 (2008).

[11] C. Federrath, Magnetic field amplification in turbulent astrophysical plasmas, J. Plasma Phys. **82**, 535820601 (2016).

[12] F. Rincon, Dynamo theories, J. Plasma Phys. **85**, 205850401 (2019).

[13] P. Tzeferacos, A. Rigby, A. F. A. Bott, A. R. Bell, R. Bingham, A. Casner, F. Cattaneo, E. M. Churazov, J. Emig, F. Fiuza, C. B. Forest, J. Foster, C. Graziani, J. Katz, M. Koenig, C. K. Li, J. Meinecke, R. Petrasso, H. S. Park, B. A. Remington, J. S. Ross, D. Ryu, D. Ryutov, T. G. White, B. Reville, F. Miniati, A. A. Schekochihin, D. Q. Lamb, D. H. Froula, and G. Gregori, Laboratory evidence of dynamo amplification of magnetic fields in a turbulent plasma, Nat. Commun. **9**, 591 (2018).

[14] A. P. Kazantsev, Enhancement of a magnetic field by a conducting fluid, Soviet J. Exper. Theor. Phys. **26**, 1031 (1968).

[15] Ya. B. Zel'dovich, A. A. Ruzmaikin, S. A. Molchanov, and D. D. Sokoloff, Kinematic dynamo problem in a linear velocity field, J. Fluid Mech. **144**, 1 (1984).

[16] S. Childress and A. D. Gilbert, *Stretch, Twist, Fold: The Fast Dynamo*, Lecture Notes in Physics Vol. 37 (Springer-Verlag, Berlin Heidelberg, 1995).

[17] A. Seta, P. Bhat, and K. Subramanian, Saturation of Zeldovich stretch-twist-fold map dynamos, J. Plasma Phys. **81**, 395810503 (2015).

[18] A. A. Ruzmaikin, D. D. Sokoloff, and A. M. Shukurov (Eds.), *Astrophysics and Space Science Library*, Vol. 133 (Springer, Berlin, 1988).

[19] R. M. Kulsrud and S. W. Anderson, The spectrum of random magnetic fields in the mean field dynamo theory of the Galactic magnetic field, Astrophys. J. **396**, 606 (1992).

[20] A. Shukurov and D. Sokoloff, Astrophysical dynamos, in *Les Houches, Session LXXXVIII, Dynamos*, Vol. 88, edited by P. Cardin and L. F. Cugliandolo (Elsevier, Amsterdam, 2007), pp. 251–299.

[21] R. Pakmor, F. A. Gómez, R. J. J. Grand, F. Marinacci, C. M. Simpson, V. Springel, D. J. R. Campbell, C. S. Frenk, T. Guillet, C. Pfrommer, and S. D. M. White, Magnetic field formation in the Milky Way like disk galaxies of the Auriga project, Mon. Not. R. Astron. Soc. **469**, 3185 (2017).

[22] A. H. Minter and S. R. Spangler, Observation of turbulent fluctuations in the interstellar plasma density and magnetic field on spatial scales of 0.01 to 100 parsecs, Astrophys. J. **458**, 194 (1996).
[23] A. Seta, Cosmic ray propagation in turbulent galactic magnetic fields, Ph.D. thesis, Newcastle University, 2019.
[24] A. Ruzmaikin, D. Sokoloff, and A. Shukurov, The dynamo origin of magnetic fields in galaxy clusters, Mon. Not. R. Astron. Soc. **241**, 1 (1989).
[25] K. Subramanian, A. Shukurov, and N. E. L. Haugen, Evolving turbulence and magnetic fields in galaxy clusters, Mon. Not. R. Astron. Soc. **366**, 1437 (2006).
[26] P. Bhat and K. Subramanian, Fluctuation dynamos and their Faraday rotation signatures, Mon. Not. R. Astron. Soc. **429**, 2469 (2013).
[27] F. Vazza, G. Brunetti, M. Brüggen, and A. Bonafede, Resolved magnetic dynamo action in the simulated intracluster medium, Mon. Not. R. Astron. Soc. **474**, 1672 (2018).
[28] F. Cattaneo, On the origin of magnetic fields in the quiet photosphere, Astrophys. J. **515**, L39 (1999).
[29] J. Pietarila Graham, R. Cameron, and M. Schüssler, Turbulent small-scale dynamo action in solar surface simulations, Astrophys. J. **714**, 1606 (2010).
[30] P. J. Bushby and B. Favier, Mesogranulation and small-scale dynamo action in the quiet Sun, Astron. Astrophys. **562**, A72 (2014).
[31] M. Rempel, Numerical simulations of quiet sun magnetism: On the contribution from a small-scale dynamo, Astrophys. J. **789**, 132 (2014).
[32] Ya. B. Zeldovich, A. A. Ruzmaikin, and D. D. Sokoloff, *The Almighty Chance* (World Scientific, Singapore, 1990).
[33] A. A. Schekochihin, S. C. Cowley, S. F. Taylor, J. L. Maron, and J. C. McWilliams, Simulations of the small-scale turbulent dynamo, Astrophys. J. **612**, 276 (2004).
[34] S. L. Wilkin, C. F. Barenghi, and A. Shukurov, Magnetic Structures Produced by the Small-Scale Dynamo, Phys. Rev. Lett. **99**, 134501 (2007).
[35] A. Shukurov, A. P. Snodin, A. Seta, P. J. Bushby, and T. S. Wood, Cosmic rays in intermittent magnetic fields, Astrophys. J. Lett. **839**, L16 (2017).
[36] A. Seta, A. Shukurov, T. S. Wood, P. J. Bushby, and A. P. Snodin, Relative distribution of cosmic rays and magnetic fields, Mon. Not. R. Astron. Soc. **473**, 4544 (2018).
[37] T. A. Enßlin and C. Vogt, Magnetic turbulence in cool cores of galaxy clusters, Astron. Astrophys. **453**, 447 (2006).
[38] M. Meneguzzi, U. Frisch, and A. Pouquet, Helical and Nonhelical Turbulent Dynamos, Phys. Rev. Lett. **47**, 1060 (1981).
[39] Nils Erland L. Haugen, A. Brandenburg, and W. Dobler, Simulations of nonhelical hydromagnetic turbulence, Phys. Rev. E **70**, 016308 (2004).
[40] J. Cho and D. Ryu, Characteristic lengths of magnetic field in magnetohydrodynamic turbulence, Astrophys. J. **705**, L90 (2009).
[41] F. Cattaneo and S. M. Tobias, Dynamo properties of the turbulent velocity field of a saturated dynamo, J. Fluid Mech. **621**, 205 (2009).
[42] C. Federrath, G. Chabrier, J. Schober, R. Banerjee, R. S. Klessen, and D. R. G. Schleicher, Mach Number Dependence of Turbulent Magnetic Field Amplification: Solenoidal Versus Compressive Flows, Phys. Rev. Lett. **107**, 114504 (2011).
[43] B. Favier and P. J. Bushby, Small-scale dynamo action in rotating compressible convection, J. Fluid Mech. **690**, 262 (2012).
[44] S. Sur, C. Federrath, D. R. G. Schleicher, R. Banerjee, and R. S. Klessen, Magnetic field amplification during gravitational collapse—Influence of turbulence, rotation, and gravitational compression, Mon. Not. R. Astron. Soc. **423**, 3148 (2012).
[45] A. Beresnyak, Universal Nonlinear Small-Scale Dynamo, Phys. Rev. Lett. **108**, 035002 (2012).
[46] C. Federrath, J. Schober, S. Bovino, and D. R. G. Schleicher, The turbulent dynamo in highly compressible supersonic plasmas, Astrophys. J. **797**, L19 (2014).
[47] S. Sur, P. Bhat, and K. Subramanian, Faraday rotation signatures of fluctuation dynamos in young galaxies, Mon. Not. R. Astron. Soc. **475**, L72 (2018).

[48] S. Boldyrev and F. Cattaneo, Magnetic-Field Generation in Kolmogorov Turbulence, Phys. Rev. Lett. **92**, 144501 (2004).
[49] A. A. Schekochihin, N. E. L. Haugen, A. Brandenburg, S. C. Cowley, J. L. Maron, and J. C. McWilliams, The onset of a small-scale turbulent dynamo at low magnetic Prandtl numbers, Astrophys. J. **625**, L115 (2005).
[50] A. A. Schekochihin, A. B. Iskakov, S. C. Cowley, J. C. McWilliams, M. R. E. Proctor, and T. A. Yousef, Fluctuation dynamo and turbulent induction at low magnetic Prandtl numbers, New J. Phys. **9**, 300 (2007).
[51] A. B. Iskakov, A. A. Schekochihin, S. C. Cowley, J. C. McWilliams, and M. R. E. Proctor, Numerical Demonstration of Fluctuation Dynamo at Low Magnetic Prandtl Numbers, Phys. Rev. Lett. **98**, 208501 (2007).
[52] A. Brandenburg, N. E. L. Haugen, Xiang-Yu Li, and K. Subramanian, Varying the forcing scale in low Prandtl number dynamos, Mon. Not. R. Astron. Soc. **479**, 2827 (2018).
[53] https://github.com/pencil-code.
[54] It is also common to define the hydrodynamic and magnetic Reynolds number with respect to the forcing wave number instead of the driving length scale. Then the Reynolds numbers are smaller by a factor 2π than the values we quote.
[55] P. Bhat and K. Subramanian, Fluctuation dynamo at finite correlation times and the Kazantsev spectrum, Astrophys. J. **791**, L34 (2014).
[56] P. Bhat and K. Subramanian, Fluctuation dynamos at finite correlation times using renewing flows, J. Plasma Phys. **81**, 395810502 (2015).
[57] A. Vincent and M. Meneguzzi, The spatial structure and statistical properties of homogeneous turbulence, J. Fluid Mech. **225**, 1 (1991).
[58] C. Federrath, On the universality of supersonic turbulence, Mon. Not. R. Astron. Soc. **436**, 1245 (2013).
[59] A. H. Waelkens, A. A. Schekochihin, and T. A. Enßlin, Probing magnetic turbulence by synchrotron polarimetry: Statistics and structure of magnetic fields from Stokes correlators, Mon. Not. R. Astron. Soc. **398**, 1970 (2009).
[60] F. Cattaneo, D. W. Hughes, and E.-J. Kim, Suppression of Chaos in a Simplified Nonlinear Dynamo Model, Phys. Rev. Lett. **76**, 2057 (1996).
[61] Eun-jin Kim, Nonlinear dynamo in a simplified statistical model, Phys. Lett. A **259**, 232 (1999).
[62] A. A. Schekochihin, S. C. Cowley, G. W. Hammett, J. L. Maron, and J. C. McWilliams, A model of nonlinear evolution and saturation of the turbulent MHD dynamo, New J. Phys. **4**, 84 (2002).
[63] K. Subramanian, Unified Treatment of Small- and Large-Scale Dynamos in Helical Turbulence, Phys. Rev. Lett. **83**, 2957 (1999).
[64] K. Subramanian, Hyperdiffusion in Nonlinear Large- and Small-Scale Turbulent Dynamos, Phys. Rev. Lett. **90**, 245003 (2003).
[65] S. I. Braginskii, Transport processes in a plasma, Rev. Plasma Phys. **1**, 205 (1965).
[66] L. Malyshkin and R. M. Kulsrud, Magnetized turbulent dynamos in protogalaxies, Astrophys. J. **571**, 619 (2002).
[67] A. Brandenburg, R. L. Jennings, Å. Nordlund, M. Rieutord, R. F. Stein, and I. Tuominen, Magnetic structures in a dynamo simulation, J. Fluid Mech. **306**, 325 (1996).
[68] J. Mason, F. Cattaneo, and S. Boldyrev, Dynamic Alignment in Driven Magnetohydrodynamic Turbulence, Phys. Rev. Lett. **97**, 255002 (2006).
[69] S. Servidio, W. H. Matthaeus, and P. Dmitruk, Depression of Nonlinearity in Decaying Isotropic MHD Turbulence, Phys. Rev. Lett. **100**, 095005 (2008).
[70] M. K. Verma, Statistical theory of magnetohydrodynamic turbulence: Recent results, Phys. Rep. **401**, 229 (2004).
[71] R. Kumar, M. K. Verma, and R. Samtaney, Energy transfers and magnetic energy growth in small-scale dynamo, Europhys. Lett. **104**, 54001 (2013).
[72] F. Plunian, R. Stepanov, and P. Frick, Shell models of magnetohydrodynamic turbulence, Phys. Rep. **523**, 1 (2013).
[73] M. K. Verma and R. Kumar, Dynamos at extreme magnetic Prandtl numbers: Insights from shell models, J. Turbul. **17**, 1112 (2016).

[74] D. A. St-Onge, M. W. Kunz, J. Squire, and A. A. Schekochihin, Fluctuation dynamo in a weakly collisional plasma, arXiv:2003.09760.
[75] P. H. Roberts, *An Introduction to Magnetohydrodynamics* (Longmans, Green, and Co., London, 1967).
[76] H. Minkowski, Volumen und oberfläche, Math. Ann. **57**, 447 (1903).
[77] J. Schmalzing, T. Buchert, A. L. Melott, V. Sahni, B. S. Sathyaprakash, and S. F. Shandarin, Disentangling the cosmic web. I. Morphology of isodensity contours, Astrophys. J. **526**, 568 (1999).
[78] T. Leung, N. Swaminathan, and P. A. Davidson, Geometry and interaction of structures in homogeneous isotropic turbulence, J. Fluid Mech. **710**, 453 (2012).
[79] V. Zhdankin, S. Boldyrev, J. C. Perez, and S. M. Tobias, Energy dissipation in magnetohydrodynamic turbulence: Coherent structures or "nanoflares"? Astrophys. J. **795**, 127 (2014).
[80] A. Kapahtia, P. Chingangbam, S. Appleby, and C. Park, A novel probe of ionized bubble shape and size statistics of the epoch of reionization using the contour Minkowski tensor, J. Cosmol. Astropart. Phys. **2018**, 011 (2018).
[81] S. Bag, R. Mondal, P. Sarkar, S. Bharadwaj, and V. Sahni, The shape and size distribution of H II regions near the percolation transition, Mon. Not. R. Astron. Soc. **477**, 1984 (2018).
[82] S. Bag, R. Mondal, P. Sarkar, S. Bharadwaj, T. Roy Choudhury, and V. Sahni, Studying the morphology of HI isodensity surfaces during reionization using Shapefinders and percolation analysis, Mon. Not. R. Astron. Soc. **485**, 2235 (2019).
[83] J. Schmalzing and K. M. Gorski, Minkowski functionals used in the morphological analysis of cosmic microwave background anisotropy maps, Mon. Not. R. Astron. Soc. **297**, 355 (1998).
[84] S. Bharadwaj, V. Sahni, B. S. Sathyaprakash, S. F. Shandarin, and C. Yess, Evidence for filamentarity in the Las Campanas Redshift survey, Astrophys. J. **528**, 21 (2000).
[85] I. Makarenko, A. Fletcher, and A. Shukurov, 3D morphology of a random field from its 2D cross-section, Mon. Not. R. Astron. Soc. **447**, L55 (2015).
[86] P. K. Joby, P. Chingangbam, T. Ghosh, V. Ganesan, and C. D. Ravikumar, Search for anomalous alignments of structures in Planck data using Minkowski tensors, J. Cosmol. Astropart. Phys. **2019**, 009 (2019).
[87] M. W. Crofton, On the theory of local probability, applied to straight lines drawn at random in a plane: The methods used being also extended to the proof of certain new theorems in the integral calculus, Philos. Trans. R. Soc. London I **158**, 181 (1868).
[88] D. Legland, K. Kiêu, and M-F. Devaux, Computation of Minkowski measures on2D and 3D binary images, Image Anal. Stereol. **2**, 83 (2011).
[89] V. Sahni, B. S. Sathyaprakash, and S. F. Shandarin, Shapefinders: A new shape diagnostic for large-scale structure, Astrophys. J. Lett. **495**, L5 (1998).
[90] K. Subramanian, Can the turbulent galactic dynamo generate large-scale magnetic fields? Mon. Not. R. Astron. Soc. **294**, 718 (1998).
[91] For $\mathrm{Pr_M} > 1$, fast magnetic reconnection at very high $\mathrm{Re_M}$ might alter the shape of the structures [12]; see Sec. VI for further discussion.
[92] G. L. Eyink, Stochastic flux freezing and magnetic dynamo, Phys. Rev. E **83**, 056405 (2011).
[93] Nils Erland L. Haugen, A. Brandenburg, and A. J. Mee, Mach number dependence of the onset of dynamo action, Mon. Not. R. Astron. Soc. **353**, 947 (2004).
[94] A. Brandenburg, Nonlinear small-scale dynamos at low magnetic Prandtl numbers, Astrophys. J. **741**, 92 (2011).
[95] G. Sahoo, P. Perlekar, and R. Pandit, Systematics of the magnetic-Prandtl-number dependence of homogeneous, isotropic magnetohydrodynamic turbulence, New J. Phys. **13**, 013036 (2011).
[96] François Rincon, F. Califano, A. A. Schekochihin, and F. Valentini, Turbulent dynamo in a collisionless plasma, Proc. Natl. Acad. Sci. U.S.A. **113**, 3950 (2016).
[97] D. A. St-Onge and M. W. Kunz, Fluctuation dynamo in a collisionless, weakly magnetized plasma, Astrophys. J. **863**, L25 (2018).